Resonant Second-Order Nonlinear Terahertz Response of Gallium Arsenide

Ahmed Ghalgaoui, Klaus Reimann, Michael Woerner,* and Thomas Elsaesser
Max-Born-Institut für Nichtlineare Optik und Kurzzeitspektroskopie, 12489 Berlin, Germany

Christos Flytzanis
Laboratoire Pierre Aigrain, École Normale Supérieure, 75231 Paris, France

Klaus Biermann
Paul-Drude-Institut für Festkörperelektronik, 10117 Berlin, Germany

(Received 12 September 2018; revised manuscript received 29 October 2018; published 27 December 2018)

The second-order nonlinear response of bulk GaAs in the terahertz (THz) range is mapped via the THz field emitted after near-infrared interband excitation. Phase-resolved THz detection reveals three nonlinear processes occurring in parallel, the Raman excitation of transverse optical phonons, the creation of coherent polarizations on heavy-hole–light-hole transitions, and the generation of displacive shift currents with a THz spectrum controlled by the near-infrared optical phase. Theoretical calculations reproduce the data and demonstrate the interband character of shift currents.

DOI: 10.1103/PhysRevLett.121.266602

Zinc blende semiconductors display large second-order optical nonlinearities $\chi^{(2)}$, which allow for the generation of strong nonlinear polarizations $\mathbf{P}^{(2)} = \epsilon_0 \chi^{(2)} : \mathbf{EE}$ [1–3]. In nonlinear optics, second-order polarizations are widely exploited for frequency conversion such as second-harmonic generation or difference-frequency mixing. To avoid absorption losses, these three-wave interaction schemes are typically implemented under nonresonant conditions with the optical frequencies of the interacting fields in the transparency range of the material. Tuning the frequencies to electronic and/or phonon resonances allows for an enhancement of the nonlinearities by the transition dipoles involved, and opens new nonlinear interaction pathways. Impulsive Raman scattering generates coherent transverse optical (TO) phonons, which are both Raman and infrared active [4]. This process is schematically shown in Fig. 1(b) for the band structure of GaAs. Another example is impulsively generated coherences on dipole-allowed heavy-hole–light-hole transitions [5].

Resonant excitation with photon energies above the fundamental band gap generates so-called shift currents of electron and holes via the bulk photovoltaic effect, which is of second order in the optical field [6–8]. For shift currents in bulk GaAs, both mechanisms based on intraband [9–12] and interband [13–18] currents have been considered. In the *intraband* picture, the shift current is assigned to photoexcited electron and hole distributions asymmetric in k space giving rise to a current along a particular direction. As the band structure and the photogenerated carrier distributions are inversion symmetric in k space, even for the zinc blende structure without inversion symmetry in real space (time-reversal symmetry of the Hamiltonian leads to Kramer doublets, [19]), a symmetry-breaking interaction mechanism among the carriers is required for generating a net intraband current [9–12]. Intraband theories predict a highly structured optical generation spectrum of the shift current, for which some limited experimental evidence has been presented [10,11].

The *interband* picture (first introduced in Ref. [14]) invokes a spatial charge separation mechanism upon excitation of electron-hole pairs as schematically shown in Fig. 1(a) [13–18]. We consider the electron density $|\Psi_{\mathrm{VB/CB}}|^2$ of a valence-band (VB) wave packet and a conduction-band (CB) wave packet, plotted along the space diagonal of the cubic unit cell. Upon excitation of a VB wave packet into the CB with an identical wave packet envelope [20], the center of gravity of the electron density shifts to the left [red and blue curves in Fig. 1(a)]. According to band-structure calculations [21–23], eigenstates at the maximum of the VB concentrate the electron density on the As anions whereas those at the minimum of the CB on the Ga cations [18]. This is a consequence of the Coulomb potential of the nuclei (black curve), which has deeper minima on the As anions than on the Ga cations. As a result, a shift current occurs, which is proportional to both the electron-hole (eh) generation (recombination) rate dn_{eh}/dt and the involved displacement $\Delta\mathbf{r}_{\mathrm{VB}\leftrightarrow\mathrm{CB}}$ of the electronic charge (e: elementary charge):

$$j_{\mathrm{shift}} = e\Delta\mathbf{r}_{\mathrm{VB}\leftrightarrow\mathrm{CB}} \cdot \frac{dn_{\mathrm{eh}}}{dt}. \tag{1}$$

So far, the theoretical and limited experimental work on shift currents in GaAs has mainly addressed photon

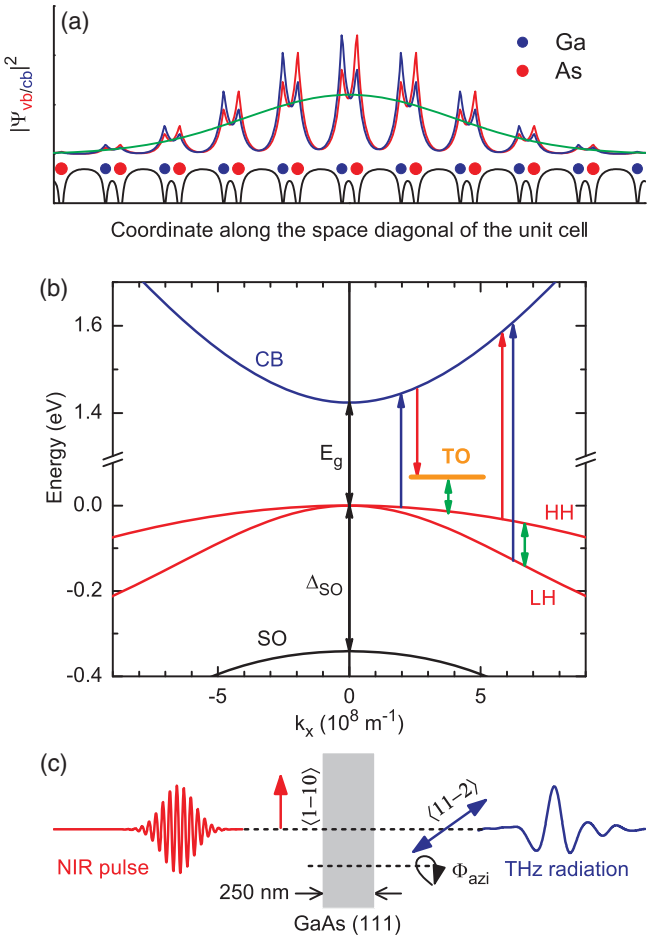

FIG. 1. (a) Electron density $|\Psi_{VB/CB}|^2$ of VB (red curve) and CB (blue curve) wave packets in GaAs with an identical envelope (green curve) plotted along the space diagonal of the cubic unit cell. Black: Coulomb potential near the As (red) and Ga (blue) atoms. (b) Calculated band structure of GaAs along k_x showing the split-off (SO), light-hole (LH), heavy-hole (HH) VBs and the CB together with the dipole-allowed transitions. Additionally, there are also transitions possible involving TO phonons (orange level). (c) Experimental geometry. Linearly polarized (red arrow) NIR pulses excite resonantly a 250-nm thick, (111)-oriented GaAs film. The nonlinearly emitted THz radiation is detected in the orthogonal polarization direction (blue arrow). The sample can be rotated by the azimuthal angle Φ_{azi} around its ⟨111⟩ axis.

energies close to the fundamental band gap. In contrast, the second-order nonlinear response in the terahertz (THz) frequency range has remained mainly unexplored. This range is particularly interesting as the overall nonlinearity should reflect the interplay of contributions from TO phonons [4], from coherences on transitions between the anisotropic valence bands [5], and from shift-current components [15,17]. In this Letter, we present a systematic experimental and theoretical study of the resonantly excited second-order THz response of bulk GaAs. A (111)-oriented sample is excited by femtosecond pulses centered at different photon energies between 1.35 and 1.9 eV. The nonlinear response is mapped via the sample's THz emission. A fully phase-resolved detection of the emitted THz field reveals three distinct contributions originating from coherent shift currents with a partial intervalence band component, coherent heavy-hole–light-hole polarizations, and coherent TO phonons. The shift currents can be tailored by changing the optical phase in the near-infrared excitation process. The observed behavior is fully reproduced by detailed theoretical calculations based on a pseudopotential band structure.

In the experiments, tunable femtosecond pulses were generated at a 1 MHz repetition rate using an optical parametric amplifier (Opera-F; Light Conversion) pumped by an Yb-based laser system (Monaco; Coherent). The compressed pulses of 20–40 fs duration are split into pump pulses (pulse energy 0.5 μJ, Gaussian shape, beam diameter 3 mm) exciting the sample and probe pulses for electro-optic (EO) sampling of the emitted THz radiation. Determined by the duration of the optimally compressed probe pulses, electro-optic sampling can measure frequencies up to 18 THz. Most experiments were performed with a 10 μm-thick ⟨110⟩-oriented ZnTe layer attached to a thick inactive ⟨100⟩-oriented ZnTe substrate. For detection within the reststrahlen band of ZnTe between 5.3 and 6.2 THz, complementary measurements are performed with a GaP crystal (thickness 200 μm, reststrahlen band 10.9 to 12.1 THz) [24]. In the pump arm we introduced additional dispersive optics to control the frequency chirp of the pump pulses. All measurements are performed in a nitrogen atmosphere at ambient temperature ($T = 300$ K).

The sample is a 250-nm-thick ⟨111⟩-oriented GaAs layer [Fig. 1(c)] mounted on a glass substrate. The ⟨111⟩ orientation was chosen because any nonvanishing second-order nonlinearity involves all Cartesian coordinates, i.e.,

$$\chi^{(2)}_{xyz} = \chi^{(2)}_{yxz} = \chi^{(2)}_{xzy} = \chi^{(2)}_{zyx} = \chi^{(2)}_{yzx} = \chi^{(2)}_{zxy} \qquad (2)$$

In a first series of experiments the nonlinearly emitted electric field $E_{THz}(t)$ [Fig. 2(a)] was measured for different photon energies of the excitation pulses. The THz waveform shows a main subpicosecond transient followed by long-lasting oscillations. In a second series ($\hbar\omega_{ex} = 1.56$ eV), we kept the polarization geometry fixed and performed a rotation of the sample around its ⟨111⟩ axis by the azimuthal angle Φ_{azi} [Fig. 1(c)]. As a function of Φ_{azi} we observe transients of identical temporal shape but with different amplitudes of the electric field. The normalized amplitudes are shown in Fig. 2(b) (symbols) together with the expected result $E(\Phi_{azi}, t) = \cos(3\Phi_{azi})E(\Phi_{azi} = 0, t)$ according to Eq. (2).

The transients shown in Fig. 2(a) contain components of distinctly different frequencies depending on the excitation energy. To generate data in the spectral range blocked by the reststrahlen band of ZnTe (5.3–6.2 THz), we performed

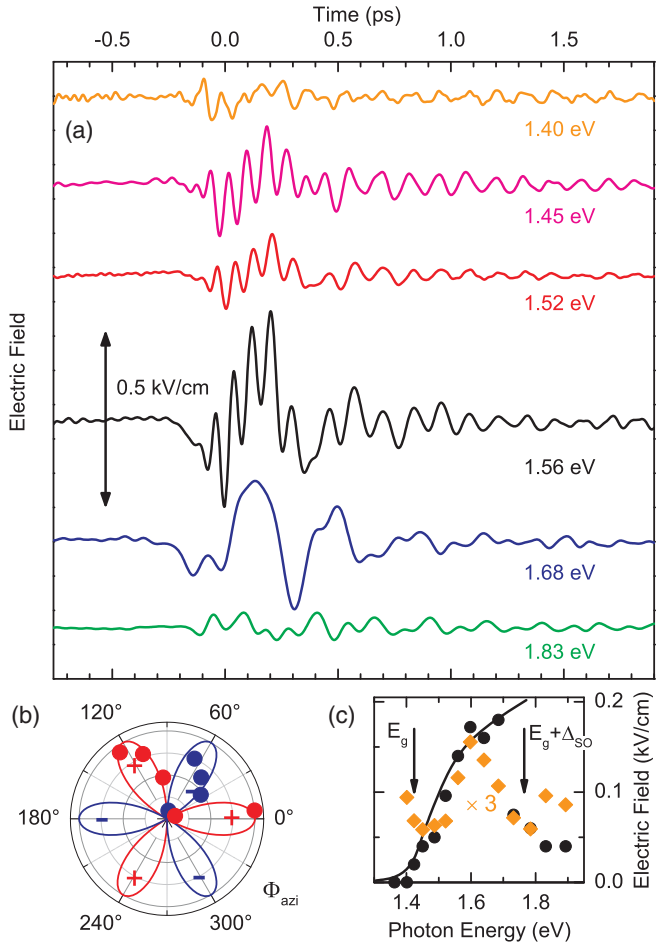

FIG. 2. (a) THz transients measured at $\Phi_{azi} = 0$ using a 10 μm-thick ZnTe crystal for electrooptic sampling at various excitation photon energies. (b) Amplitude $E(\Phi_{azi})/E(\Phi_{azi} = 0)$ (experiment: symbols, theory: solid lines) of the nonlinearly emitted electric field as a function of the azimuthal angle Φ_{azi}. (c) Electric field amplitude of the shift-current (circles) and the TO-phonon (diamonds) contributions as a function of the excitation photon energy. The solid line is the shift-current contribution from the calculation.

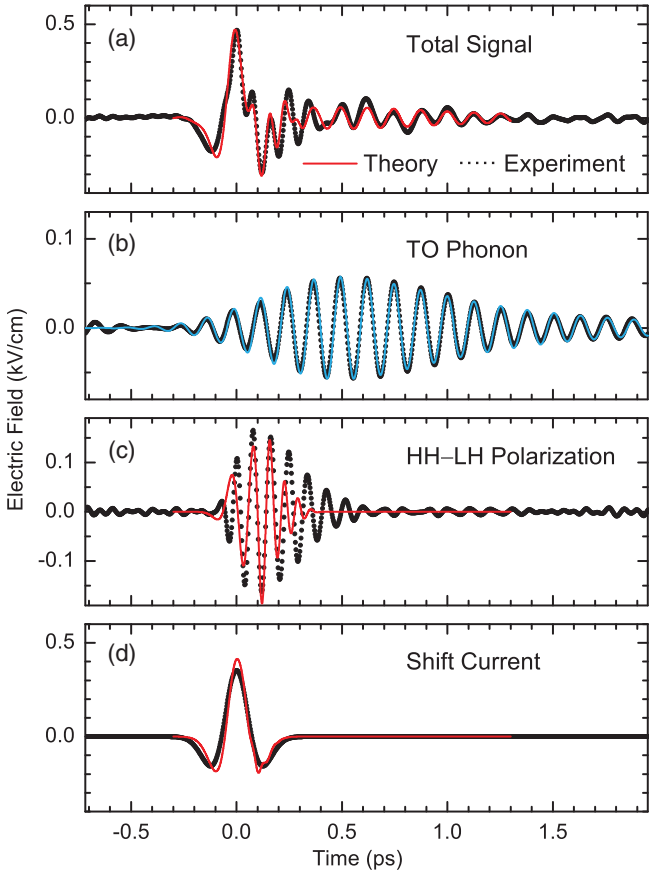

FIG. 3. (a) Nonlinearly emitted THz transient ($\hbar\omega_{ex} = 1.56$ eV, $\Phi_{azi} = 0$) reconstructed from two measurements with ZnTe and GaP electro-optic crystals (black symbols). The red line represents the corresponding theory curve. (b) TO phonon contribution to the signal found by fitting an exponentially decaying sine wave convoluted with a Gaussian (cyan curve) to the spectral peak at 8 THz [cf. Fig. 4(a)]. (c) Signal contribution due to coherent HH ↔ LH intervalence band polarizations. (d) Shift-current contribution to the nonlinear signal.

complementary measurements with a GaP crystal for EO sampling. A Fourier transform of the ZnTe and GaP data sets into the frequency domain provides the spectral amplitudes and phases of the transients. The relative spectral phases were adjusted in the spectral range covered by both measurements and the reststrahlen gap in the ZnTe spectra was bridged with the scaled spectral components from the GaP data [24]. A Fourier back transform to the time domain then gives the total signal transient plotted in Fig. 3(a).

The spectrum of the total signal transient is presented in Fig. 4(a). There are three major components with maxima at 3, 8, and 12 THz. The narrow-band emission at 8 THz stems from coherent TO phonons excited by a resonant impulsive Raman process explained in Fig. 1(b). For a 2nd-order (dipole-allowed) interaction sequence the coherent phonon amplitude is generated by the Raman process and radiates via its infrared dipole, a behavior typical for TO phonons belonging to the irreducible representation Γ_{15} of the point group $\bar{4}3m$ [4], since these phonons are both Raman and infrared active. We fitted an exponentially decaying sine wave convoluted with a Gaussian [Fig. 3(b)] to the transient in Fig. 3(a) at late times ($t > 0.5$ ps). The corresponding Fourier spectrum is shown in Fig. 4(a) (cyan line).

After subtracting the coherent TO-phonon contribution from the experimental spectrum, there are two components left with maxima at 3 and 12 THz. A Fourier back transform to the time domain provides the transients plotted in Figs. 3(c) and 3(d). They display a markedly different time structure: the high-frequency transient [Fig. 3(c)] exhibits a damped oscillatory behavior, while the low-frequency field in Fig. 3(d) follows the second time

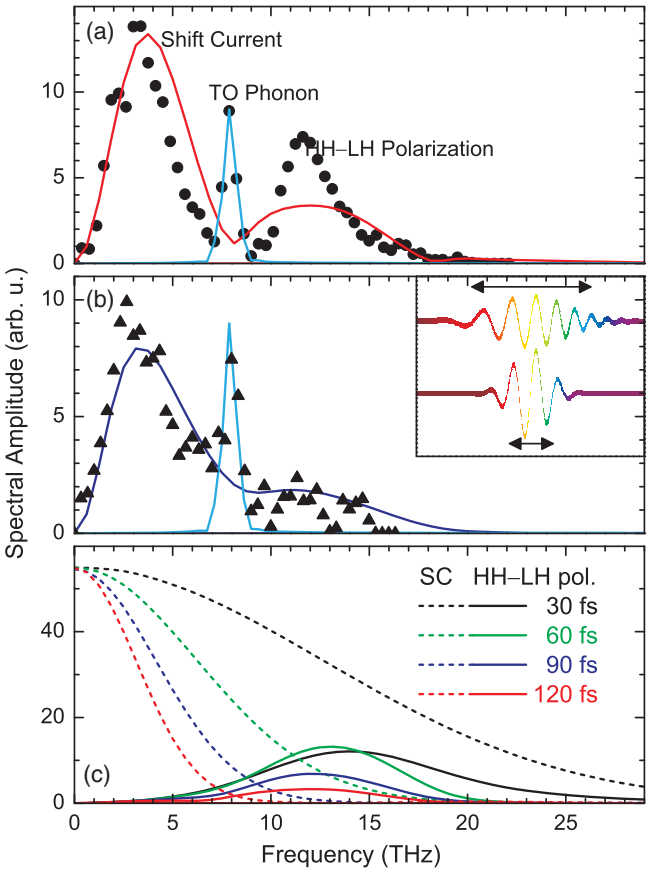

FIG. 4. (a) Dots: Fourier transform of the experimental transient shown in Fig. 3(a). Cyan curve: Fourier transform of the TO-phonon contribution in Fig. 3(b). Red curve: model calculation ($\hbar\omega_{ex} = 1.56$ eV) of the pure electronic contribution to the nonlinear signal generated by a positively chirped driving pulse with a pulse length of $\Delta t_{FWHM} = 120$ fs. (b) Experiment (symbols) and theory (blue curve) for a driving pulse with less chirp ($\Delta t_{FWHM} = 90$ fs). Inset: electric field of two differently chirped driving pulses. (c) Calculated spectra of shift-current contributions (dashed lines) and contributions due to coherent HH $\leftrightarrow$ LH polarizations (solid lines) for positively chirped driving pulses with durations as indicated.

derivative of the envelope of the near-infrared excitation pulses. It should be noted that frequency components below 1 THz (wavelength $\lambda > 300$ μm) suffer strong diffraction losses in the optical setup and, thus, are not measured.

For theoretical calculations we use a local pseudopotential band structure including spin-orbit splitting [21–23]. The pseudopotential parameters were taken from Ref. [23] apart from $V^S(\sqrt{3})$, $V^A(\sqrt{3})$, and λ^S. These three parameters were adjusted to yield the band gap ($E_g = 1.424$ eV), the spin-orbit splitting ($\Delta_{SO} = 0.341$ eV), and the heavy-hole mass in [100] direction ($0.4m_0$) at room temperature [25]. As in Ref. [23], reciprocal lattice vectors $\mathbf{G}$ with $|\mathbf{G}| \leq 22\pi/a$ were considered, resulting in 102 bands (including a factor of 2 because of spin). Using this band structure, the interaction with the external electric field is included in the velocity gauge [26]; i.e., the vector potential $\mathbf{A}(t) = \int_0^t \mathbf{E}(t')dt'$ is used. For every initial $\mathbf{k_0}$ the time dependence of the density matrix is solved with the initial condition that all valence bands are filled and all conduction bands are empty. Apart from the interaction with the electric field a phenomenological decoherence of all nondiagonal elements of the density matrix with a time constant of 250 fs [27] is included. The electric field emitted by an electron is proportional to the trace of the density matrix times the velocity operator. The total emitted field from all electrons is obtained by solving the density matrix on a grid (up to a dimension of $47 \times 47 \times 47$) of initial $\mathbf{k_0}$. The calculation does not include the interaction with phonons and excitonic effects.

The spectra of the total interband shift current calculated for the present experimental conditions are shown in Fig. 4(c). The width of the current spectra depends strongly on the frequency chirp of the near-infrared excitation pulses. Excitation by bandwidth-limited 30 fs pulses generates the widest current spectrum, while positively chirped pulses (carrier frequency increases with time) of longer duration induce currents of decreasing spectral width. Longer pulses are connected with a decrease of the carrier generation rate in Eq. (1) and a concomitant narrowing of the spectrum. This phase-sensitive behavior holds potential for steering coherent THz shift currents by controlling near-infrared optical phases, a novel perspective of optical control. Our calculations [black line in Fig. 2(c)] in line with Refs. [18,28] reproduce the shift-current contribution (circles) well up to about $\hbar\omega_{ex} = 1.7$ eV [29]. Our experimental data and those obtained earlier with narrow-band pulses [15] do not agree with the results in Ref. [10]. Consequently, this (intraband) theory has to be ruled out because it predicts a strong decrease of the shift current for photon energies above 1.46 eV (band gap + one LO-phonon energy), which is not observed. The TO-phonon contribution (diamonds) has finite values even at the band gap $\hbar\omega_{ex} = 1.4$ eV similar to the resonance behavior shown in Fig. 4 of Ref. [4].

The solid lines in Fig. 4(c) represent the spectra of currents due to coherent HH $\leftrightarrow$ LH coherences. Their frequency is determined by the HH $\leftrightarrow$ LH energy separation in the k range of optically coupled states [30]. Again, the amplitude is strongly chirp dependent and decreases with increasing pulse duration. With increasing pulse duration, the blue and red components of the driving pulse have less and less temporal overlap as sketched in the inset of Fig. 4(b), thus reducing the amplitude of the generated intervalence-band polarization.

In Fig. 4(a), the experimental spectrum (symbols) is compared with a theoretical spectrum (red curve, after removing low-frequency components due to diffraction losses as in the experiment). This spectrum was calculated with a positively chirped driving pulse of 120 fs duration, i.e., 4 times longer than its bandwidth-limited counterpart

of 30 fs. We find a good agreement with the experiment in both the spectral and the time domain [Fig. 3(a)]. The relevance of frequency chirp is supported by a second experiment and calculation for a driving pulse with less chirp ($\Delta t_{\mathrm{FWHM}} = 90$ fs) as shown in Fig. 4(b). Theory predicts a destructive interference between the coherent HH $\leftrightarrow$ LH polarizations and the shift current around 8 THz, i.e., the sharp dip in the red curve shown in Fig. 4(a). It should be emphasized that the picture of optically generated interband currents accounts quantitatively for the observed nonlinear behavior.

In conclusion, we presented a systematic experimental and theoretical study of the second-order nonlinear terahertz response of gallium arsenide. In our experiments we excited a (111)-oriented thin layer of bulk GaAs with femtosecond optical pulses and monitored the coherent THz emission by electrooptic sampling. The nonlinearly emitted THz field consists of three different contributions: shift currents due to displacive electron-hole generation, coherent emission of both heavy-hole–light-hole polarizations and resonance-Raman excited coherent TO phonons. The experiments show polarization properties in full agreement with the symmetry of the second-order conductivity tensor and are in agreement with theoretical calculations based on a pseudopotential band structure calculation. For a large positive chirp the intervalence-band contribution spectrally separates from the shift-current contribution.

We acknowledge financial support by the Deutsche Forschungsgemeinschaft: RE 806/9-1.

*woerner@mbi-berlin.de

[1] S. S. Jha and N. Bloembergen, Nonlinear optical susceptibilities in Group-IV and III-V semiconductors, Phys. Rev. **171**, 891 (1968).

[2] C. Flytzanis, Infrared dispersion of second-order electric susceptibilities in semiconducting compounds, Phys. Rev. B **6**, 1264 (1972).

[3] Y. R. Shen, *The Principles of Nonlinear Optics* (Wiley, Hoboken, NJ, 2003).

[4] R. Trommer and M. Cardona, Resonant Raman scattering in GaAs, Phys. Rev. B **17**, 1865 (1978).

[5] M. Joschko, M. Woerner, T. Elsaesser, E. Binder, T. Kuhn, R. Hey, H. Kostial, and K. Ploog, Heavy-Light Hole Quantum Beats in the Band-to-Band Continuum of GaAs Observed in 20 Femtosecond Pump-Probe Experiments, Phys. Rev. Lett. **78**, 737 (1997).

[6] A. M. Glass, D. von der Linde, and T. J. Negran, High-voltage bulk photovoltaic effect and the photorefractive process in $LiNbO_3$, Appl. Phys. Lett. **25**, 233 (1974).

[7] A. M. Glass, D. von der Linde, D. H. Auston, and T. J. Negran, Excited state polarization, bulk photovoltaic effect and the photorefractive effect in electrically polarized media, J. Electron. Mater. **4**, 915 (1975).

[8] B. I. Sturman and V. M. Fridkin, *The Photovoltaic and Photorefractive Effects in Noncentrosymmetric Materials* (Gordon and Breach, Philadelphia, 1992).

[9] V. I. Belinicher and B. I. Sturman, The photogalvanic effect in media lacking a center of symmetry, Usp. Fiz. Nauk **130**, 415 (1980) [Sov. Phys. Usp. **23**, 199 (1980)].

[10] V. I. Belinicher and V. N. Novikov, Photogalvanic effect in piezoelectrics: Quantitative theory for interband transitions in gallium arsenide, Phys. Status Solidi B **107**, 61 (1981).

[11] V. L. Alperovich, V. I. Belinicher, V. N. Novikov, and A. S. Terekhov, Photogalvanic effects investigation in gallium arsenide, Ferroelectrics **45**, 1 (1982).

[12] V. L. Al'perovich, V. I. Belinicher, A. O. Minaev, S. P. Moshchenko, and A. S. Terekhov, Ballistic photogalvanic effect at interband transitions in gallium arsenide, Fiz. Tverd. Tela (Leningrad) **30**, 3111 (1988) [Sov. Phys. Solid State **30**, 1788 (1988)].

[13] W. Kraut and R. von Baltz, Anomalous bulk photovoltaic effect in ferroelectrics: A quadratic response theory, Phys. Rev. B **19**, 1548 (1979).

[14] R. von Baltz and W. Kraut, Theory of the bulk photovoltaic effect in pure crystals, Phys. Rev. B **23**, 5590 (1981).

[15] X.-C. Zhang, Y. Jin, K. Yang, and L. J. Schowalter, Resonant Nonlinear Susceptibility Near the GaAs Band Gap, Phys. Rev. Lett. **69**, 2303 (1992).

[16] C. Aversa and J. E. Sipe, Nonlinear optical susceptibilities of semiconductors: Results with a length-gauge analysis, Phys. Rev. B **52**, 14636 (1995).

[17] D. Côté, N. Laman, and H. M. van Driel, Rectification and shift currents in GaAs, Appl. Phys. Lett. **80**, 905 (2002).

[18] F. Nastos and J. E. Sipe, Optical rectification and shift currents in GaAs and GaP response: Below and above the band gap, Phys. Rev. B **74**, 035201 (2006).

[19] C. Kittel, *Quantum Theory of Solids*, 2nd ed. (Wiley, Hoboken, 1987).

[20] B. Gu, N. H. Kwong, and R. Binder, Relation between the interband dipole and momentum matrix elements in semiconductors, Phys. Rev. B **87**, 125301 (2013).

[21] M. L. Cohen and T. K. Bergstresser, Band structures and pseudopotential form factors for fourteen semiconductors of the diamond and zinc-blende structures, Phys. Rev. **141**, 789 (1966).

[22] J. R. Chelikowsky and M. L. Cohen, Electronic Structure of GaAs, Phys. Rev. Lett. **32**, 674 (1974).

[23] J. R. Chelikowsky and M. L. Cohen, Nonlocal pseudopotential calculations for the electronic structure of eleven diamond and zinc-blende semiconductors, Phys. Rev. B **14**, 556 (1976); Erratum, Phys. Rev. B **30**, 4828(E) (1984).

[24] A. Leitenstorfer, S. Hunsche, J. Shah, M. C. Nuss, and W. H. Knox, Detectors and sources for ultrabroadband electro-optic sampling: Experiment and theory, Appl. Phys. Lett. **74**, 1516 (1999).

[25] O. Madelung, *Semiconductors—Basic Data*, 2nd ed., edited by O. Madelung (Springer, Berlin, 1996).

[26] R. R. Schlicher, W. Becker, J. Bergou, and M. O. Scully, Interaction Hamiltonian in quantum optics or: $\mathbf{p}\cdot\mathbf{A}$ vs $\mathbf{E}\cdot\mathbf{r}$ revisited, in *Proceedings of the NATO ASI on Quantum Electrodynamics and Quantum Optics, Boulder, Colorado, 1983*, edited by A. O. Barut (Plenum, New York, 1984), pp. 405–441.

[27] This value is taken from the experimentally observed decay of the HH-LH coherence [Fig. 3(c)]. Decoherence is due to carrier-carrier and carrier-phonon scattering.

[28] M. D. Sturge, Optical absorption of gallium arsenide between 0.6 and 2.75 eV, Phys. Rev. **127**, 768 (1962); Erratum, Phys. Rev. **129**, 2835(E) (1963).

[29] The origin of the discrepancy between experiment and theory above $\hbar\omega_{\mathrm{ex}} = 1.7$ eV is unclear and requires further theoretical work.

[30] For excitation energies above 1.56 eV, the frequency of the HH-LH coherences is beyond the experimental detection limit of 18 THz [Fig. 2(a)].